Fluorescent Dyes

Rhodamines with a Chloronicotinic Acid Fragment for Live Cell Superresolution STED** Microscopy

Florian Grimm,[a] Jasmin Rehman,[a] Stefan Stoldt,[b] Taukeer A. Khan,[b] Jan Gero Schlötel,[c] Shamil Nizamov,[a] Michael John,[d] Vladimir N. Belov,*[b] and Stefan W. Hell[b]

Abstract: Formylation of 2,6-dichloro-5-*R*-nicotinic acids at C-4 followed by condensation with 3-hydroxy-*N*,*N*-dimethylaniline gave analogs of the popular TAMRA fluorescent dye with a 2,6-dichloro-5-R-nicotinic acid residues (R = H, F). The following reaction with thioglycolic acid is selective, involves only one chlorine atom at the carbon between pyridine nitrogen and the carboxylic acid group and affords new rhodamine dyes absorbing at 564/ 573 nm and emitting at 584/ 597 nm (R = H/ F, in aq. PBS). Conjugates of the dyes with "small molecules" provided specific labeling (covalent and non-covalent) of organelles as well as of components of the cytoskeleton in living cells and were combined with fluorescent probes prepared from *610CP* and *SiR* dyes and applied in two-color STED microscopy with a 775 nm STED laser.

Introduction

A high demand on bright, photostable and selective fluorescent markers for optical microscopy of living matter stimulated progress in the design, synthesis and screening of the new cell permeable fluorophores.[1] The core structures are compact,[2] and the whole dye molecules have reactive centers and, in some cases, additional solubilizing groups.[3] These features and the absence of a net electrical charge, are essential for target-specific probes[4] including fluoresceins,[5] rhodamines,[6] their carbon,[6b,c,d,f] silicon[7] and germanium analogs, as well as related structures.[8] The design of the probes is focused not only on fluorescent dyes, but also includes the proper choice of linkers and ligands (small molecules) for binding (covalent or non-covalent) with biological targets. The dye-ligand conjugates were applied for selective in vivo labeling of proteins and cell organelles in neurons, human fibroblasts, U2OS, COS-7 and HeLa cells using confocal and super resolution microscopy.[3,6,7e–g,8b,9]

The structures of "live dyes" are based on a xanthene (pyronine) fluorophore and resemble "good old" 5′(6′)-carboxy-*N*,*N*,*N*′,*N*′-tetramethylrhodamine[10] (X = O, R = OH). The *meso* carbon atom of a positively charged fluorophore can react with a carboxyl group in the *ortho*-position of the pendant phenyl ring (C-3′). This leads to the equilibrium between the zwitterionic (fluorescent) and spirolactone (non-fluorescent) forms (Scheme 1). Tetramethylrhodamine (TMR) represents a very simple and attractive scaffold for construction of the new dyes. An additional carboxyl group attached to C-5′ or C-6′ is used for bioconjugation. Thus, 2′,5′- or 2′,6′-dicarboxyphenyl group (Scheme 1) remained the most conservative structural

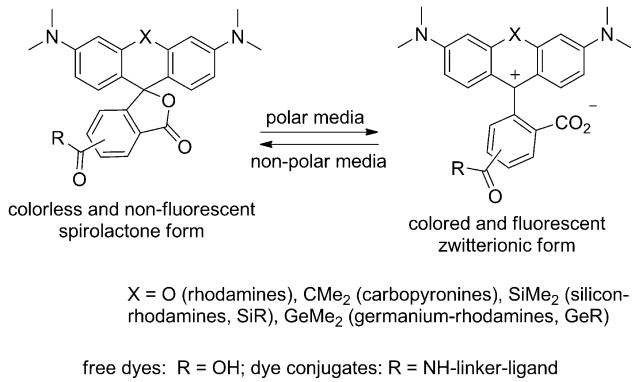

Scheme 1. Membrane-permeant fluorophores in equilibrium between non-fluorescent and fluorescent forms. For structures of *565pR*, linkers and ligands, see Scheme 2 and Figure 3.

[a] *F. Grimm, J. Rehman, Dr. S. Nizamov*
Abberior GmbH
Hans Adolf Krebs Weg 1, 37077 Göttingen (Germany)
[b] *Dr. S. Stoldt, Dr. T. A. Khan, Dr. V. N. Belov, Prof. Dr. S. W. Hell*
Department of Nanobiophotonics
Max Planck Institute for Biophysical Chemistry (MPIBPC)
Am Fassberg 11, 37077 Göttingen (Germany)
E-mail: vbelov@gwdg.de
[c] *Dr. J. G. Schlötel*
Abberior-Instruments GmbH
Hans Adolf Krebs Weg 1, 37077 Göttingen (Germany)
[d] *Dr. M. John*
Institute of Organic and Biomolecular Chemistry
Georg-August University
Tammannstr. 2, 37077 Göttingen (Germany)
[**] *STED: stimulated emission depletion*
Supporting information and the ORCID identification number(s) for the author(s) of this article can be found under: https://doi.org/10.1002/chem.202005134.

element in all successful membrane-permeant dyes and was not varied until very recently.[8, 11] Incorporation of 2,6-dichloronicotinic residue into the TMR structure represented a very simple and attractive option to prepare analogs **4**-TAMRA dye (Scheme 2) which was reported very recently and demonstrated excellent performance in fluorescent probes.[11b] Due to the presence of the (reactive) halogen atoms in the precursor compounds **4**-R (Scheme 2) we expected easy functionalization, the red shifted emission and increased $D_{0.5}$ values (see discussion below). These were the main reasons why we embarked on the synthesis and characterization of the new dyes **5**-R (R = H, F; Scheme 2) and fluorescent probes derived from them.

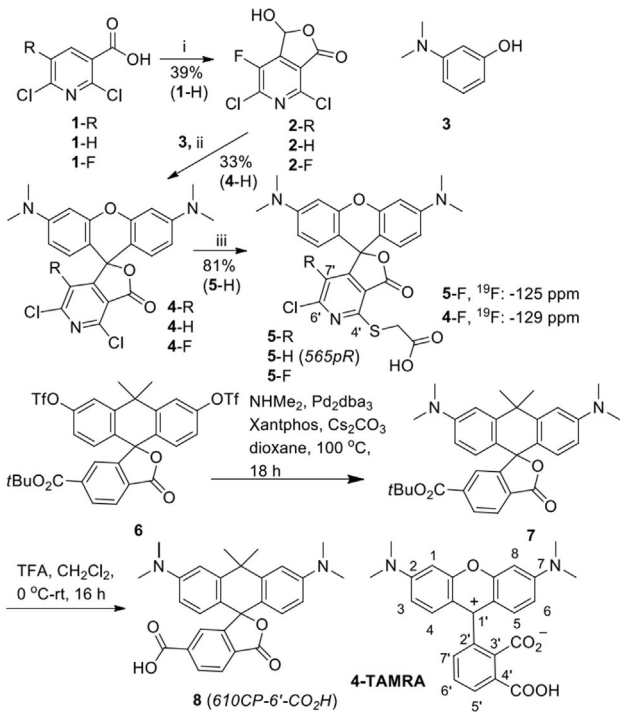

Scheme 2. Synthesis of chloropyridine-containing rhodamine dyes **5**-R as analogs of **4**-TAMRA (with the uniform numeration of the carbon atoms). Reagents and conditions: i) LDA, THF, −78 °C, 1 h; then DMF, −78 °C to RT, 1 h; ii) 1,2-dichlorbenzene, 120 °C, 3 h; iii) $HSCO_2H$, Et_3N, DMF, RT, 1 h.

Results and Discussion

Synthesis (Scheme 2) and photophysical properties of the new dyes

The commercial availability of 2,6-dichloro-5-*R*-nicotinic acids (**1**-R) allows to replace the benzoic acid residue in the classical TMR molecule by 2,6-dichloro-5-R-pyridine fragments (R = H, F) and synthesize compounds **4**-R. The reactivity of thiols in nucleophilic substitution of the activated chlorine atoms in pyridines indicated the possibility to prepare 2-chloropyridine-containing rhodamine dyes **5**-R (R = H, F). Acids **1**-R were lithiated (at O and C-4 atoms) with an excess of lithium diisopropylamide (THF, −78 °C) and then transformed into aldehydes **2**-R (existing in a cyclic form; see Supporting Information for details). Heating of compounds **2**-R (R = H, F) with 3-(*N*,*N*-dimethylamino)phenol (**3**) was performed in the presence of air oxygen, in order to provide oxidation of the intermediate leuco-forms (the structures not shown) to dyes **4**-R. We tried various solvents (propionic acid, toluene, trifluoroethanol; with and without acidic catalysts), but only in dichlorobenzene rhodamines **4**-R were formed in moderate yield. Careful addition of thioglycolic acid to the solutions of compounds **4**-R in DMF at room temperature resulted in selective substitution of the chlorine between the carboxylic acid group and the nitrogen atom[12] and resulted in the new fluorescent dyes **5**-R bearing a short linker and the second carboxylate. The NMR spectra of rhodamines **4**-R and **5**-R displayed broad signals at + 25 °C; probably due to protonation of the pyridine nitrogen. At elevated temperatures (75 °C) the spectra could be interpreted, and the signals assigned. For compound **5**-H, the position of the carboxymethylthio group is supported by the absence of the NOE between the CH_2S protons and any other protons in the molecule. For compound **5**-F, the position of the carboxymethylthio group is supported by the absence of the NOE between the CH_2S group and the aromatic protons attached to C-4 and C-5 of the xanthen moiety. For compound **5**-F, the position of the carboxymethylthio group is additionally supported by the relatively small high-field shift of ^{19}F signal: −129 ppm in **4**-F and −125 ppm in **5**-F (+4 ppm). If the carboxymethylthio group were attached to C-6′, we would expect much stronger high-field shift of 27–31 ppm.[13] Having dyes **5**-R at hand we studied their photophysical properties (Table 1, Figure 1 and S2) prepared conjugates with small molecules (Figure 3) and tested them as fluorescent probes for imaging of various organelles in fixed and living cells (Figures 2–5 and Supporting Information). As a reference, we chose the structurally and spectrally similar dye **4**-TAMRA (Scheme 2) which performed exceptionally well in STED microscopy.[11b] As a supplementary dye we used carbopyronine *610CP-6′-CO₂H*[6c] (**8**) whose versatility in bioconjugates[6b, d, 9c] and spectral properties allowed to combine it with **4**-TAMRA[11b[and dyes **5**-R in labelling and superresolution STED microscopy. The wide applicability of *610CP* prompted to optimize the synthesis of this dye. Inspired by the published transformations,[11b[we proved that

Table 1. Photophysical properties of dyes measured in aqueous PBS at pH 7.5

Dye	Absorption λ_{max} [nm] (ε, [M^{-1} cm^{-1}])[a]	Emission λ_{max} [nm] (Φ_{fl})[b]	$D_{0.5}$[c]	Lifetime[d] [ns]
5-H (*565pR*)	564 (90 000)	589 (0.31)	24	2.2
5-F	double: 529/ 573 (57 000)	597 (0.29)	15	2.0
4-TAMRA[e]	551 (78 000)	573 (0.41)	14	2.0
610CP-6′-COOH[f]	609 (100 000)	634 (0.59)	36	3.1

[a] ε—extinction coefficient. [b] Φ_{fl}—fluorescence quantum yield (absolute value). [c] Dielectrical constant of dioxane (D = 2)—water (D = 80) mixture, in which the fluorescent form (Scheme 1) is present to 50 % of its maximal possible concentration (in pure water). [d] Lifetime of the excited state. [e] Scheme 2; data from ref. [11b]. [f] Figure 3; data from ref. [6c].

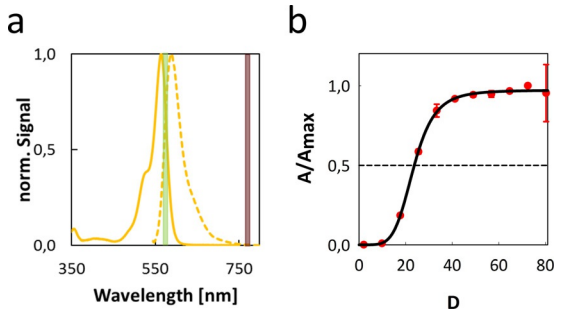

Figure 1. a) Normalized absorption (solid line) and emission (dashed line) spectra of pyridine-containing rhodamine **5**-H (*565pR*) in PBS at pH 7.5. Green bar shows excitation at 561 nm and red bar represent 775 nm STED laser. b) Normalized absorption (A/A_{max}) at λ_{max} of **5**-H (*565pR*) plotted vs. dielectric constant (*D*) of dioxane-water mixtures. $D_{0.5}$ values (Table 1) correspond to the intersection of interpolated graphs with $A/A_{max} = 0.5$ line.

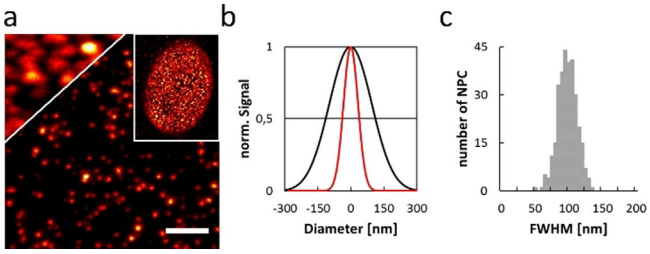

Figure 2. Confocal and STED microscopy (indirect immunofluorescence) of a nuclear pore complex (NPC) protein NUP98 in fixed Vero cell labeled with dye **5**-H (565pR): a) STED and confocal (upper left corner) images of NPC with a confocal overview of the whole nucleus (upper right corner), scale bar 1 μm; b) example of an line profile of one NPC under confocal (black line) and STED (red line) conditions; the Gaussian fits gave full-width-at-half-maximum (FWHM) of 220 nm for confocal and 86 nm for STED image; c) distribution of FWHM values (N = 309) under STED conditions. Confocal and STED images were acquired using a pulsed 561 nm excitation laser (average power at focal plane: 2.8 μW, 40 MHz). For STED images a pulsed 775 nm STED laser (average power at focal plane: 60 mW, 40 MHz; pulse length: 1.1 ns).

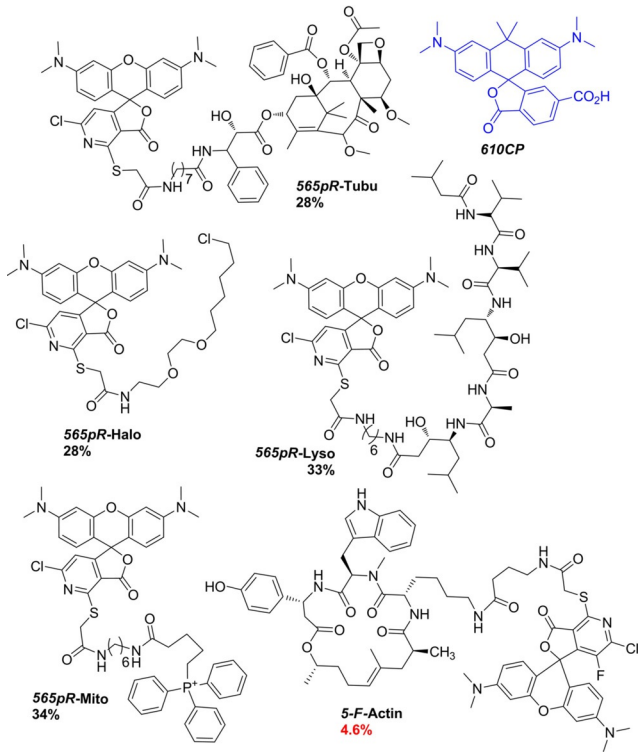

Figure 3. Chemical structures of fluorescent probes based on dye **5**-H (**5**-F for actin) connected via amide bounds and linkers with ligands (recognition units) for tubulin (cabazitaxel), lysomes (pepstatin A), mitochondria [(4-carboxybutyl)triphenylphosphonium] and HaloTag fusion protein (HaloTag amine O2). The values of the fluorescence quantum yields (in aq. PBS) are given. Blue: structure of *610CP-6′-COOH* (carbopyronine) dye incorporated into tubulin probe (see Figure S6) and used in two-color STED imaging.

bis-triflate **6** can be used as a universal precursor to carbopyronine dyes with 6′-COOH group, including *580CP and 610CP* (see Scheme 2 and Supporting Information).

The photophysical properties of these dyes (Table 1) are given in aqueous buffer at pH 7.5; under conditions relevant to living cells. The main absorption and emission bands of dye **5**-H (*565pR*) are shown in Figure 1. Small bathochromic and bathofluoric shifts (13 nm and 16 nm) observed for *565pR* in comparison with 4-TAMRA are explained by the presence of the electron-acceptor pyridine ring with the chlorine substituent. Further red shifts were observed for compound **5**-F (Figure S2), and are explained by the presence of the fluorine atom.[14] All dyes in Table 1 (except **5**-F) feature very similar band shapes and Stokes shifts of 20–30 nm.

Dye **5**-F has an absorption band in aqueous PBS with two maxima at 529 and 573 nm, so that the extinction coefficient measured at the maximum is lower, but the oscillator strength (proportional to the band area) is roughly the same, as for compound **5**-H. Importantly, the emission bands of the new dyes **5**-R extend to the far-red region, and STED superresolution microscopy is possible with the most widely used 775 nm laser (see below).

The presence of organic solvents shifts the absorption and emission spectra of compounds **5**-R to the blue spectral region, but only slightly. For example, in methanol and aqueous acetonitrile the absorption/ emission maxima of **5**-H are found at 556/ 580 and 559/ 586 nm, respectively; the ε-values are lower than in aqueous solutions (70 000 and 73 000 in methanol and aq. acetonitrile, respectively). For compound **5**-F, the absorption/ emission maxima in methanol are found at 569 nm and 591 nm, respectively, while the extinction coefficient (75 000 $M^{-1}cm^{-1}$; one band with a shoulder typical for xanthene dyes) is higher than the value measured in aqueous PBS solution (see Table 1). Lower extinction coefficients in organic solvents are due to the presence of the colorless and non-emissive "closed" forms in the equilibrium with the "open", zwitterionic, colored and fluorescent isomers (Scheme 1). As a measure of the equilibrium between "open" and "closed" forms (Scheme 1), we use the parameter $D_{0.5}$: the dielectric constant of the dioxane-water mixture at which the normalized absorption A/A_{max} (or $\varepsilon/\varepsilon_{max}$) of the dye is equal to 50% of the maximal value observed within the entire dioxane-water gradient.[3,6b,d,e,f,9c,11b] The absorption spectra in dioxane-water solutions were recorded, with water content varying from 0 to 100% and dielectric constant (*D*) changing from 2.0

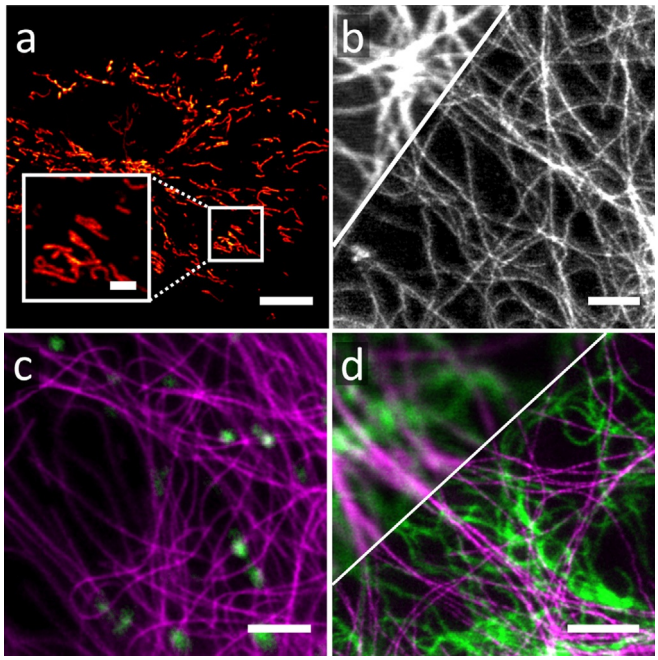

Figure 4. Imaging of cellular structures and organelles in living cells stained with *565pR* probes (for structures, see Figure 3): a) confocal image of mitochondria network in a living human fibroblast labeled with *565pR*-Mito with a close-up (white frame; scale bar 2 μm) of a selected region; scale bar: 10 μm; b) STED and confocal (upper left corner) microscopy images of tubulin network in a living U2OS cell stained with *565pR*-Tubu; scale bar: 2 μm; c) two-color image of lysosomes (confocal) stained with *565pR*-Lyso (green) and tubulin network (STED) stained with *610CP*-Tubu in a living human fibroblast; scale bar: 2 μm; d) two-color STED and confocal (upper left corner) images of a monoclonal vimentin-Halo expressing U2OS cell; vimentin and tubulin were stained with a *565pR*-Halo (green) and *610CP*-Tubu (magenta) probes, respectively; scale bar 2 μm. Confocal and STED images were recorded with Facility Line (a–c) or Expert Line microscopes (d) equipped with a pulsed 561 nm (for *565pR*-probes) and 640 nm (for *610CP*-Tubu) excitation lasers, respectively, and a pulsed 775 nm STED laser (repetition rate: 40 MHz; pulse duration: 1.1 ns). The color separation in c was enabled by *rainbow detection*.

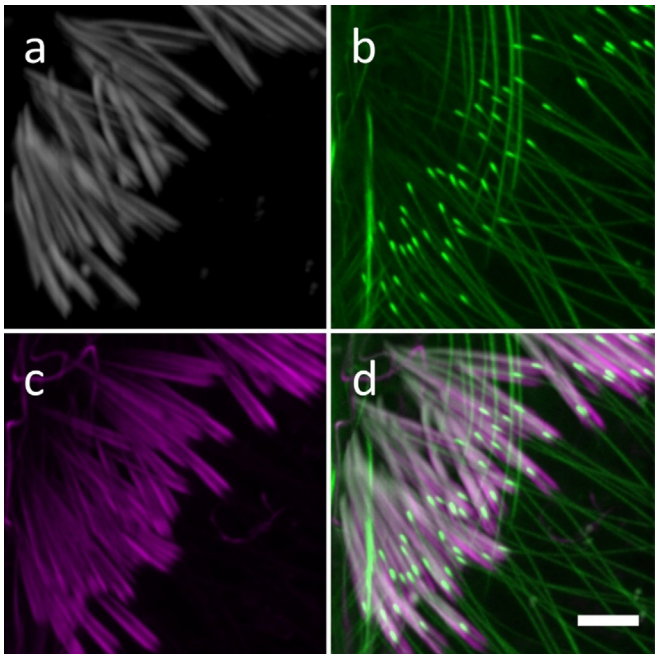

Figure 5. Multicolor confocal volume-image (*z*-projection, 45 frames) of sperm bundles inside *Drosophila melanogaster* adult testis (*ex vivo*). a) DNA stained with Hoechst ("grey"), b) tubulin stained with *565pR*-Tubu ("green"), c) actin cones stained with *SiR*-Actin ("magenta"). d) Merge of three channels shown in a–c. Images were recorded with excitation lasers 405 nm, 561 nm and 640 nm (for Hoechst, *565pR* and *SiR* dyes, respectively) on a Facility Line microscope (Abberior Instruments GmbH) equipped with rainbow detection module. Scale bar 10 μm.

to 80.4, respectively (Figure 1). This series of spectra allow to evaluate the response of the dyes to the solvent polarity, calculate and directly compare the $D_{0.5}$ parameters of the dyes, even if their absorption and emission spectra are different. **4**-TAMRA and compound **5**-F (surprisingly!) have the lowest $D_{0.5}$ values (14–15).[11b] Introduction of the chlorosubstituted pyridine ring (an acceptor group) favors the closed-ring lactone form (due to destabilization of the positive charge on the *meso* carbon atom opposite to oxygen: C-1′) and increases $D_{0.5}$ value of *565pR* to 24 (Table 1). It is not clear, why the presence of an additional electron-acceptor (fluorine) in compound **5**-F does not increase the $D_{0.5}$ value even further. The $D_{0.5}$ value of *610CP* is higher (36), because the $>C(CH_3)_2$ center disrupts the conjugation and does not stabilize the positive charge on a fluorophore so efficient, as the oxygen atom does. Notably, high $D_{0.5}$ values are required but not sufficient for fluorogenicity (fluorogenic response) of the dyes and their conjugates (increase in fluorescence intensity upon selective binding with the target). Thus, all non-fluorogenic dyes (**4**-TAMRA, *565pR*) have low values of $D_{0.5}$, while higher values of $D_{0.5}$ (e.g., 64 for *SiR* as a bench-mark dye[7a-g] or carbopyronines[6b,c]) suggest that the dye and its conjugates may be fluorogenic. The relatively low $D_{0.5}$ values observed for the reported dyes are typical for all rhodamines without halogen atoms (F, Cl) in the *N*-alkyl groups (2,2,2-trifluorethyl) and/or xanthene fluorophore (C-3, C-6).[3,6c] This may be a limitation typical for rhodamines, if only fluorogenic probes are required (e.g., for "no wash" experiments). Thus, low $D_{0.5}$ values may help to exclude the dyes from screening and save work in their synthesis. However, if the fluorogenic effect is caused by the ligand (due to pi-pi stacking of two aromatic systems),[6b] then the dyes with low $D_{0.5}$ values can be considered and screened.

Fluorescent conjugates and imaging performance of the dyes

Indirect immunofluorescence is a standard approach for evaluation of the imaging performance under confocal and STED conditions. The STED wavelengths in the near IR region −775 nm for Abberior Instruments and Leica Microsystems, 765 nm for PicoQuant—are present in all commercial STED microscopes, because in this spectral region the absorbance of cells and tissues is low. Therefore, as in the previous studies, most of red-emitting dyes are designed for the use with 775 nm or 765 nm STED lasers. To prepare bioconjugates, compounds **5**-H and **5**-F (Scheme 2) were converted into NHS esters (for experimental details, see Supporting Information) and conjugated with proteins or small molecules (ligands)

(Figure 3), as recognition units for subcellular structures in living specimen. The fluorescence quantum yields of compounds in Figure 3 were measured in aqueous PBS and varied in the range 28–34% for all conjugates of *565pR* and was lower (4.6%) for ***5**-F-Actin* probe (probably due to stronger aggregation of the fluorinated dye). The better performing dye **5**-H (*565pR*) was conjugated to goat anti-rabbit IgG secondary antibodies and tested in fixed cells for staining of nuclear porin 98 (NUP98) protein (Figure 2). In a fluorescence microscope, the NUP98 protein stained with fluorescent dyes looks like bright dots of similar sizes. Under confocal and STED conditions *565pR* provided bright images with low background. The fluorescent images of 309 NUP98 complexes were analyzed, and the optical resolution assessed as full-width-at-half-maximum (FWHM) of the emission profiles of individual objects and gave an average value of 96 nm. For that we used a pulsed 775 nm STED laser with an average power of 60 mW, 40 MHz measured at the focal plane and a pulse length of 1.1 ns. Although, the dye *565pR* has a particularly weak absorbance at 775 nm (Figure 1), a relatively strong improvement in optical resolution was observed.

The *565pR* dye conjugates (Figure 3) were prepared and tested in living human fibroblast and U2OS cells (Figures 4–6 and S3–S6).

We used microscopes manufactured by Abberior Instruments GmbH (Expert and Facility Line), in order to get confocal and STED images. The new model (Facility Line) has a pair of gradient-coated light filters coupled with the so-called "rainbow detection module", in order to freely define the edges of the detection windows in the range between 400 and 800 nm. This feature enables more freedom in choosing fluorescent markers primarily according to their biolabeling performance, with fewer limitations due to spectral overlap and predefined detection intervals. All conjugates shown in Figure 3 gave specific and bright staining of mitochondria (*565pR*-Mito), tubulin (*565pR*-Tubu), lysosomes (*565pR*-Lyso) and vimentin (*565pR*-Halo). Most of the mitochondria-selective fluorescent probes contain the positively charged and lipophilic triphenylphosphonium residue.[15] According to this principle, we used 5-(triphenylphosphonium)pentanoic acid, linked it with *565pR* via 1,6-diaminohexane spacer and thus prepared *565pR*-Mito (Figure 4a). For staining of microtubules (Figure 4b and S3), we prepared a fluorescent conjugate of the anticancer drug cabazitaxel. Along with docetaxel and larotaxel, cabazitaxel binds (non-covalently) to tubulin and facilitates microtubule formation. It was shown[6f] that cabazitaxel[16] often provides superior images than docetaxel which was used in most of the earlier studies. Then we tested the lysosome probe (*565pR*-Lyso). Lysosomes are cell organelles containing hydrolytic enzymes which digest unwanted substances in the cytoplasm. As a ligand we used pepstatin A, which inhibits cathepsin D—a major lysosomal aspartic endopeptidase—and which has been previously incorporated into the fluorescent probes.[6f,7f,8b,17] We used 1,6-diaminohexane as a linker binding the carboxyl groups of pepstatin A and *565pR* dye. For better visualization we co-stained the microtubulin filaments with a probe containing dye *610CP* providing high specificity and fluorogenic behavior in many bioconjugates.[6b,c,d,f,9c] Different excitation lasers and the optimized light distribution between two acquisition channels enabled very efficient color separation and negligible crosstalk, though the emission maxima of *565pR* and *610CP* were separated only by 40–45 nm and band shapes were very similar (for optical spectra and excitation wavelength, see Supporting Information). Since the dye *610CP* can be also exited with 561 nm laser light, we collected the emission of *565pR*-Lyso in the range from 571 nm to 600 nm, cutting off the possible emission of *610CP*. The detection channel for the probe *610CP*-Tubu was set from 650 nm to 725 nm. Therefore, the two channels in Figure 4c and S6 has been nicely separated using the rainbow detection giving the opportunity to see movement of the lysosomes along the microtubule filaments (Figure 4c and S6). The binding to mitochondria (*565pR*-Mito), tubulin (*565pR*-Tubu), and lysosomes (*565pR*-Lyso) was non-covalent, while the vimentin probe (*565pR*-Halo) was applied in living U2OS cells expressing a vimentin-HaloTag fusion protein[9c] and provided covalent binding (Figure 4d and S4, S5). We also used *610CP*-Tubu for co-staining. For imaging we used the Abberior Instruments expert line equipped with the detection windows of 580 nm −630 nm and 650 nm to 720 nm. The color separation of both probes was still possible, although the weak emission from *610CP*-Tubu was observed in the detection window from 580 nm −630 nm.

For staining of actin, we used conjugate of **5**-F with the established actin ligand des-bromo-des-methyljasplakinolide (bound via L-lysine residue and 6-aminohexanoic acid linkers with a fluorescent dye).[18,19] Actin protein plays a crucial role in cellular function and motility.[20] It can be present either as a monomer (G-actin; globular) or, upon polymerization, it may form filaments (F-actin): flexible fibers with a diameter of 4–7 nm and length of up to several micrometers. In living cells, both forms of actin are present in equilibrium; they are essential for the proper mobility and contraction of cells during cell division, cell motility, cytokinesis, vesicle and organelle movement, cell signaling, as well as the establishment and maintenance of cell junctions and cell shape. We tested the actin probe based on dye **5**-F (**5**-F-Actin in Figure 3) in concentrations of 0.5 μM, 1 μM and 5 μM on living and fixed U2OS cells. The specific and bright staining was observed only for fixed cells, with concentration of 1 μM being the optimal one (see Figure S7). No significant staining was observed with living cells (also for the structural analog incorporating compound **5**-H). It is possible to explain these results by cell impermeability: the low $D_{0.5}$ values (Table 1) indicate that the dyes are zwitterionic, and the zwitterions do not cross the membranes as good as unpolar spirolactone forms do (Scheme 1). Another explanation may be based on the presence of the pyridine ring which might inhibit binding with native F-actin. The STED effect demonstrated by the dye **5**-F in Figure S7 is strong; it is explained by the red-shifted emission band of **5**-F (emission maximum 597 nm) compared to the dye **5**-H (589 nm; Table 1), which already showed quite remarkable resolution improvement in response to the STED laser (Figure 2).

To extend the scope of labeling, we stained sperm bundles inside *Drosophila melanogaster* adult testis (*ex vivo*) with fluo-

rescent probes *565pR*-Tubu and *SiR*-Actin.[7e] Figure 6 shows the specificity of vital tubulin (green) and actin (magenta) labeling (confocal mode) referenced by the position of DNA (grey). It illustrates the highly dynamic nature, uniform direction, and characteristic morphology of sperm bundles and actin cones inside *Drosophila melanogaster* adult testis, revealed even in *ex vivo* imaging.

The thickness and dynamic behavior of actin filaments makes them an attractive object for observation with superresolution optical microscopy.[6d,18–20] Figure 5 shows confocal and STED images of tubulin fibers stained with *565pR*-Tubu (green) and actin stained with *610CP*-Actin[6d,18] (magenta) in a *Drosophila melanogaster* wild type egg chamber (*ex vivo*). Observing the confocal counterpart, we cannot exclude co-localization of these structures. The STED images were acquired with an Abberior Instruments (Facility Line) microscope according to the optical settings given in Figure 6 and mentioned above. Remarkably, even in deeper stacks of the tissue stained with the two probes *565pR*-Tubu and *610CP*-Actin, STED imaging was possible and increased the optical resolution of the fluorescent structures. Now, it was clearly seen that the filaments of tubulin and actin did not co-localize.

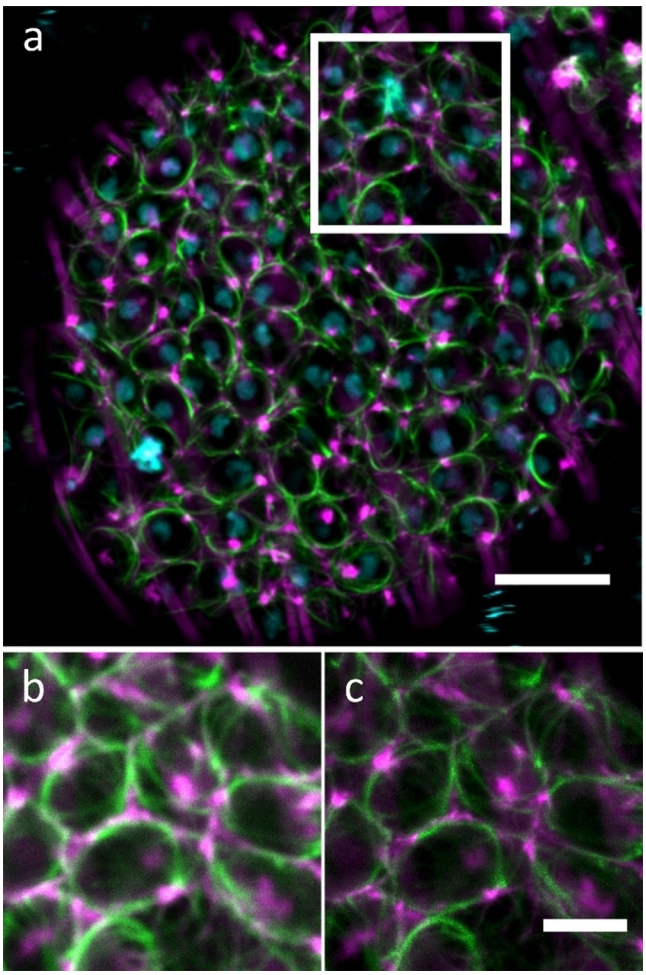

Figure 6. Confocal and STED images of *Drosophila melanogaster* wild type egg chamber (*ex vivo*). a) Three color image of DNA (cyan) stained with Hoechst, tubulin (green) stained with *565pR*-Tubu and actin (magenta) stained with *610CP*-Actin probes. b) confocal image of a chosen area in a). c) STED image of a chosen area in a). Images were recorded with a facility line (Abberior Instruments GmbH) equipped with excitation lasers 405 nm, 561 nm and 640 nm (for Hoechst, *565pR* and *610CP* dyes, respectively), a pulsed 775 nm STED laser (repetition rate: 40 MHz; pulse duration: 1.1 ns) and rainbow detection. Scale bar 10 μm (in a) and 2 μm (in b and c).

Conclusions

Two fluorescent dyes related to the popular X-carboxy-tetramethylrhodamine (X-HO_2C-TMR; $x = 4, 5, 6$), but with a 6-chloronictonic acid residue and a carboxymethylthio linker, were prepared and characterized by absorption and emission spectra. The $D_{0.5}$ value for dye **5**-H is somewhat higher than that of the structurally related **4**-TAMRA, and this suggests higher cell-permeability of the probes based on **5**-H dye. The emission maxima of the new dyes **5**-H and **5**-F are far from 775 nm (STED wavelength), but both dyes showed remarkable STED effect and substantially improved the optical resolution in fluorescence microscopy of fixed and living cells. To demonstrate that, the dyes were conjugated with secondary antibodies and small molecules: a taxol, pepstaine A, (ω-aminoalkyl)triphenylphosphonium bromide, Halo Tag amine, jasplakinolide derivative. We showed that introduction of a thiol linker is regiospecific, and only one chlorine atom (between the carboxylic acid residue and the pyridine-nitrogen) is substituted. The new fluorescent probes were tested in living cells and in a tissue of *drosophila melanogaster* and showed specific staining of the targets. The dye **5**-H has been combined with "a red-shifted" carbopyronine *610CP-6′-COOH* (whose synthesis was optimized) and used in two-color staining experiments. Although the emission spectra of *610CP* and **5**-H are very close, color separation was possible with the two detection windows of 580–630 nm and 650–720 nm. An even better separation was achieved by using the so-called "rainbow detection", when the detection boarders were varied and set individually.

Acknowledgements

The authors are grateful to Dr. Holm Frauendorf and co-workers for measuring HRMS (Institut für organische und biomolekulare Chemie der Georg-August-Universität Göttingen). We thank Dr. Leonard Drees for providing wild type *Drosophila melanogaster*. For the help with STED microscopy and scientific discussions, we thank Dr. Christian A. Wurm (Abberior Instruments GmbH). We acknowledge the financial support by Bundesministerium für Bildung und Foschung: grants nr. 13N14120 to F.G. and J.R. and 13N14122 to S.W.H. Open access funding enabled and organized by Projekt DEAL.

Conflict of interest

The authors declare no conflict of interest.

Keywords: dyes/pigments · fluorescence · fluorescent probes · scanning probe microscopy

[1] J. B. Grimm, A. N. Tkachuk, L. Xie, H. Choi, B. Mohar, N. Falco, K. Schaefer, R. Patel, Q. Zheng, Z. Liu, J. Lippincott-Schwartz, T. A. Brown, L. D. Lavis, *Nat. Methods* **2020**, *17*, 815 – 821.
[2] a) L. Galas, T. Gallavardin, M. Bénard, A. Lehner, D. Schapman, A. Lebon, H. Komuro, P. Lerouge, S. Leleu, X. Franck, *Chemosensors* **2018**, *6*, 40; b) T. Ikeno, T. Nagano, K. Hanaoka, *Chem. Asian J.* **2017**, *12*, 1435 – 1446; c) E. Kozma, P. Kele, *Org. Biomol. Chem.* **2019**, *17*, 215 – 233.
[3] A. N. Butkevich, V. N. Belov, K. Kolmakov, V. V. Sokolov, H. Shojaei, S. C. Sidenstein, D. Kamin, J. Matthias, R. Vlijm, J. Engelhardt, S. W. Hell, *Chem. Eur. J.* **2017**, *23*, 12114 – 12119.
[4] H. Zhu, J. Fan, J. Du, X. Peng, *Acc. Chem. Res.* **2016**, *49*, 2115 – 2126.
[5] a) J. B. Grimm, T. A. Brown, A. N. Tkachuk, L. D. Lavis, *ACS Cent. Sci.* **2017**, *3*, 975 – 985; b) K. Hirabayashi, K. Hanaoka, T. Takayanagi, Y. Toki, T. Egawa, M. Kamiya, T. Komatsu, T. Ueno, T. Terai, K. Yoshida, M. Uchiyama, T. Nagano, Y. Urano, *Anal. Chem.* **2015**, *87*, 9061 – 9069.
[6] a) F. Bottanelli, E. B. Kromann, E. S. Allgeyer, R. S. Erdmann, S. Wood Baguley, G. Sirinakis, A. Schepartz, D. Baddeley, D. K. Toomre, J. E. Rothman, J. Bewersdorf, *Nat. Commun.* **2016**, *7*, 780; b) J. Bucevičius, J. Keller-Findeisen, T. Gilat, S. W. Hell, G. Lukinavičius, *Chem. Sci.* **2019**, *10*, 1962 – 1970; c) A. N. Butkevich, G. Y. Mitronova, S. C. Sidenstein, J. L. Klocke, D. Kamin, D. N. H. Meineke, E. D'Este, P.-T. Kraemer, J. G. Danzl, V. N. Belov, S. W. Hell, *Angew. Chem. Int. Ed.* **2016**, *55*, 3290 – 3294; *Angew. Chem.* **2016**, *128*, 3350 – 3355; d) R. Gerasimaitė, J. Seikowski, J. Schimpfhauser, G. Kostiuk, T. Gilat, E. D'Este, S. Schnorrenberg, G. Lukinavičius, *Org. Biomol. Chem.* **2020**, *18*, 2929 – 2937; e) F. Grimm, S. Nizamov, V. N. Belov, *ChemBioChem* **2019**, *20*, 2248 – 2254; f) G. Lukinavičius, G. Y. Mitronova, S. Schnorrenberg, A. N. Butkevich, H. Barthel, V. N. Belov, S. W. Hell, *Chem. Sci.* **2018**, *9*, 3324 – 3334.
[7] a) M. Fu, Y. Xiao, X. Qian, D. Zhao, Y. Xu, *Chem. Commun.* **2008**, *23*, 1780 – 1782; b) E. Kim, K. S. Yang, R. J. Giedt, R. Weissleder, *Chem. Commun.* **2014**, *50*, 4504 – 4507; c) Y. Koide, Y. Urano, K. Hanaoka, T. Terai, T. Nagano, *ACS Chem. Biol.* **2011**, *6*, 600 – 608; d) Y. Koide, Y. Urano, K. Hanaoka, W. Piao, M. Kusakabe, N. Saito, T. Terai, T. Okabe, T. Nagano, *J. Am. Chem. Soc.* **2012**, *134*, 5029 – 5031; e) G. Lukinavičius, L. Reymond, E. D'Este, A. Masharina, F. Göttfert, H. Ta, A. Güther, M. Fournier, S. Rizzo, H. Waldmann, C. Blaukopf, C. Sommer, D. W. Gerlich, H.-D. Arndt, S. W. Hell, K. Johnsson, *Nat. Methods* **2014**, *11*, 731 – 733; f) G. Lukinavičius, L. Reymond, K. Umezawa, O. Sallin, E. D'Este, F. Göttfert, H. Ta, S. W. Hell, Y. Urano, K. Johnsson, *J. Am. Chem. Soc.* **2016**, *138*, 9365 – 9368; g) G. Lukinavičius, K. Umezawa, N. Olivier, A. Honigmann, G. Yang, T. Plass, V. Mueller, L. Reymond, I. R. Corrêa Jr, Z.-G. Luo, C. Schultz, E. A. Lemke, P. Heppenstall, C. Eggeling, S. Manley, K. Johnsson, *Nat. Chem.* **2013**, *5*, 132 – 139; h) T. E. McCann, N. Kosaka, Y. Koide, M. Mitsunaga, P. L. Choyke, T. Nagano, Y. Urano, H. Kobayashi, *Bioconjugate Chem.* **2011**, *22*, 2531 – 2538; i) T. Pastierik, P. Šebej, J. Medalová, P. Štacko, P. Klán, *J. Org. Chem.* **2014**, *79*, 3374 – 3382; j) P. Shieh, M. S. Siegrist, A. J. Cullen, C. R. Bertozzi, *Proc. Natl. Acad. Sci. USA* **2014**, *111*, 5456 – 5461; k) B. Wang, X. Chai, W. Zhu, T. Wang, Q. Wu, *Chem. Commun.* **2014**, *50*, 14374 – 14377; l) T. Wang, Q.-J. Zhao, H.-G. Hu, S.-C. Yu, X. Liu, L. Liu, Q.-Y. Wu, *Chem. Commun.* **2012**, *48*, 8781 – 8783; m) A. N. Butkevich, M. L. Bossi, G. Lukinavičius, S. W. Hell, *J. Am. Chem. Soc.* **2019**, *141*, 981 – 989.
[8] a) A. N. Butkevich, M. V. Sednev, H. Shojaei, V. N. Belov, S. W. Hell, *Org. Lett.* **2018**, *20*, 1261 – 1264; b) A. N. Butkevich, G. Lukinavičius, E. D'Este, S. W. Hell, *J. Am. Chem. Soc.* **2017**, *139*, 12378 – 12381; c) P. Horváth, P. Šebej, T. Šolomek, P. Klán, *J. Org. Chem.* **2015**, *80*, 1299 – 1311.
[9] a) J. B. Grimm, B. P. English, J. Chen, J. P. Slaughter, Z. Zhang, A. Revyakin, R. Patel, J. J. Macklin, D. Normanno, R. H. Singer, T. Lionnet, L. D. Lavis, *Nat. Methods* **2015**, *12*, 244 – 250; b) J. B. Grimm, A. K. Muthusamy, Y. Liang, T. A. Brown, W. C. Lemon, R. Patel, R. Lu, J. J. Macklin, P. J. Keller, N. Ji, L. D. Lavis, *Nat. Methods* **2017**, *14*, 987 – 994; c) A. N. Butkevich, H. Ta, M. Ratz, S. Stoldt, S. Jakobs, V. N. Belov, S. W. Hell, *ACS Chem. Biol.* **2017**, *13*, 475 – 480.
[10] P. L. Khanna, E. F. Ullman, *Anal. Biochem.* **1980**, *108*, 156 – 161.
[11] a) L. Wang, M. Tran, E. D'Este, J. Roberti, B. Koch, L. Xue, K. Johnsson, *Nat. Chem.* **2020**, *12*, 165 – 172; b) J. Bucevičius, G. Kostiuk, R. Gerasimaitė, T. Gilat, G. Lukinavičius, *Chem. Sci.* **2020**, *11*, 7313 – 7323.
[12] J. S. Scott, S. S. Bowker, J. deSchoolmeester, S. Gerhardt, D. Hargreaves, E. Kilgour, A. Lloyd, R. M. Mayers, W. McCoull, N. J. Newcombe, D. Ogg, M. J. Packer, A. Rees, J. Revill, P. Schofield, N. Selmi, J. G. Swales, P. R. O. Whittamore, *J. Med. Chem.* **2012**, *55*, 5951 – 5964.
[13] a) R. L. Neil, M. E. Peach, *J. Fluorine Chem.* **1972**, *1*, 257 – 267; b) G. Y. Mitronova, S. Polyakova, C. A. Wurm, K. Kolmakov, T. Wolfram, D. N. H. Meineke, V. N. Belov, M. John, S. W. Hell, *Eur. J. Org. Chem.* **2015**, 337 – 349.
[14] K. Kolmakov, E. Hebisch, T. Wolfram, L. A. Nordwig, C. A. Wurm, H. Ta, V. Westphal, V. N. Belov, S. W. Hell, *Chem. Eur. J.* **2015**, *21*, 13344 – 13356.
[15] S. Wisnovsky, E. K. Lei, S. R. Jean, S. O. Kelley, *Cell Chem. Biol.* **2016**, *23*, 917 – 927.
[16] a) S. J. Morley, Y. Qi, L. Iovino, L. Andolfi, D. Guo, N. Kalebic, L. Castaldi, C. Tischer, C. Portulano, G. Bolasco, K. Shirlekar, C. M. Fusco, A. Asaro, F. Fermani, M. Sundukova, U. Matti, L. Reymond, A. de Ninno, L. Businaro, K. Johnsson, M. Lazzarino, J. Ries, Y. Schwab, J. Hu, P. A. Heppenstall, *eLife* **2016**, *5*, 618; b) Y. Wang, F. Feng, L. Chen, H. Zhao, L. Tian, *Magn. Reson. Chem.* **2014**, *52*, 783 – 788.
[17] C.-S. Chen, W.-N. U. Chen, M. Zhou, S. Arttamangkul, R. P. Haugland, *J. Biochem. Biophys. Methods* **2000**, *42*, 137 – 151.
[18] V. N. Belov, S. Stoldt, F. Rüttger, M. John, J. Seikowski, J. Schimpfhauser, S. W. Hell, *J. Org. Chem.* **2020**, *85*, 7267 – 7275.
[19] L.-G. Milroy, S. Rizzo, A. Calderon, B. Ellinger, S. Erdmann, J. Mondry, P. Verveer, P. Bastiaens, H. Waldmann, L. Dehmelt, H.-D. Arndt, *J. Am. Chem. Soc.* **2012**, *134*, 8480 – 8486.
[20] A. J. Davidson, W. Wood, *Trends Cell Biol.* **2016**, *26*, 569 – 576.

Manuscript received: November 27, 2020
Accepted manuscript online: January 26, 2021
Version of record online: March 5, 2021

